

RSC Advances



This is an *Accepted Manuscript*, which has been through the Royal Society of Chemistry peer review process and has been accepted for publication.

Accepted Manuscripts are published online shortly after acceptance, before technical editing, formatting and proof reading. Using this free service, authors can make their results available to the community, in citable form, before we publish the edited article. This *Accepted Manuscript* will be replaced by the edited, formatted and paginated article as soon as this is available.

You can find more information about *Accepted Manuscripts* in the [Information for Authors](#).

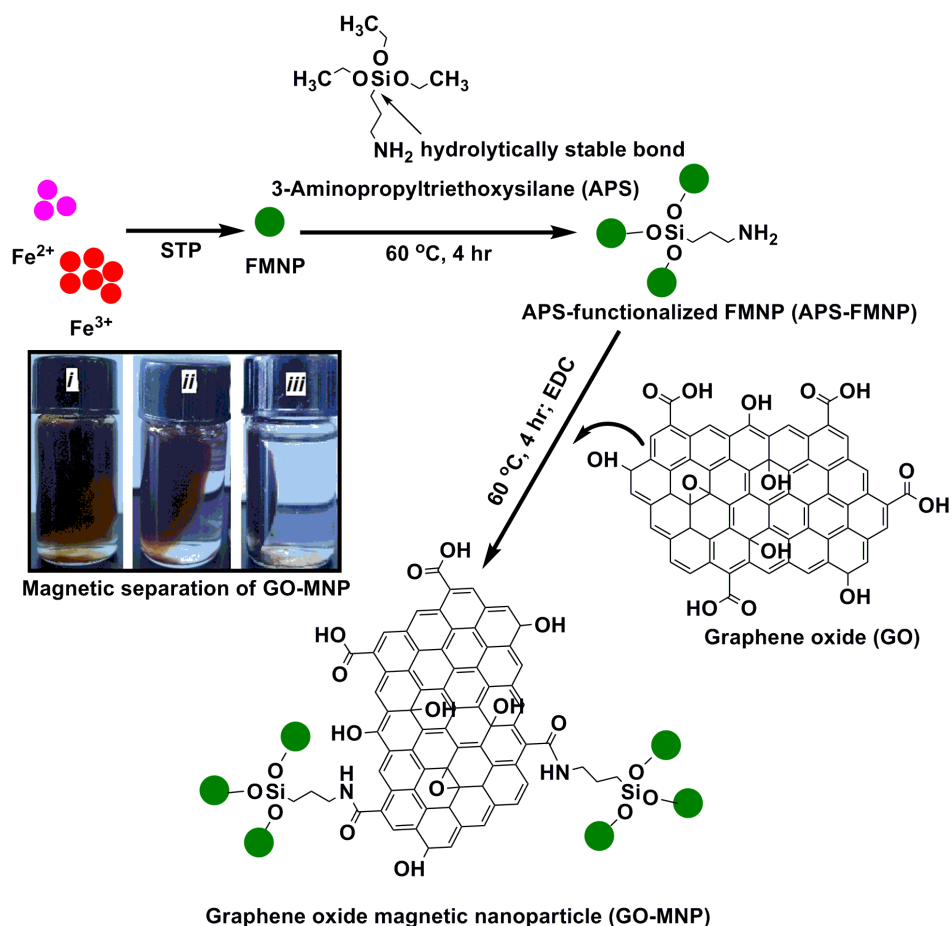
Please note that technical editing may introduce minor changes to the text and/or graphics, which may alter content. The journal's standard [Terms & Conditions](#) and the [Ethical guidelines](#) still apply. In no event shall the Royal Society of Chemistry be held responsible for any errors or omissions in this *Accepted Manuscript* or any consequences arising from the use of any information it contains.

1 **SYNTHESIS OF COVALENTLY BONDED GRAPHENE OXIDE–IRON MAGNETIC**2 **NANOPARTICLES AND ITS KINETICS OF MERCURY REMOVAL**3 Paul N. Diagboya,^{*} ^{a, b} Bamidele I. Olu-Owolabi,^b Kayode O. Adebowale^b4 ^a *National Center for Nanoscience and Technology, Beijing 100190, China*5 ^b *Department of Chemistry, University of Ibadan, Ibadan, Nigeria*6
7 *Corresponding author: Tel: +234 80 3805 2553. E-mail: pauldn2@yahoo.com8 **ABSTRACT**

9 Synergistically combined nanomaterials have been applied in various fields in materials science
10 to improve the properties of the nanocomposites. However, limited studies focused on the ability
11 of such composites for water treatment. Graphene oxide (GO)–iron oxide (Fe₃O₄) magnetic
12 nano-particles composite (GOMNP) was synthesized and used to study the Hg²⁺ adsorption
13 kinetics from aqueous solution at varying temperatures. GO was attached to magnetic
14 nanoparticles via the amine group of 3-aminopropyltriethoxysilane which was attached the
15 surface of Fe₃O₄. The GOMNP nano-composite had a Hg²⁺ adsorption capacity of 16.6 mg g⁻¹.
16 IR spectra analysis showed that hydroxyl and carboxylate functional groups were mainly
17 responsible for Hg²⁺ adsorption. Adsorption of Hg²⁺ by the GOMNP obeyed different adsorption
18 mechanisms at varying adsorption temperatures. The Elovich kinetics model described the Hg²⁺
19 adsorption data better than any other three models tested. GOMNP nano-composite is thus a
20 promising nanosorbent for Hg²⁺ removal from aqueous solutions.

21 **Keywords:** Graphene oxide; Iron magnetic (Fe₃O₄) nanoparticles; Mercury; Adsorption;
22 Kinetics.

23



1. INTRODUCTION

The adverse impact of mercury (Hg) on biota is well documented. It has been known to cause dysfunctional organs in human such as in the digestive, reproductive, cardiovascular and nervous systems, kidney, brain and eye^{1,2}. At minute concentrations of more than 6 ppb, mercury is considered very toxic^{2,3}. Hg occurs in the environment mainly in the form of methyl mercury, and in this and its other environmental forms it is not essential for plants or animals.¹ Soils and sediments are usually its final sink, and when in the environment elemental Hg gets easily methylated and it can be readily absorbed by biota in this methylated form, thus accumulating in humans via the food chain^{1,4,5}. A vivid example of mercury poisoning was seen in the Minamata incidence in the 1950s in Japan.

1 Recent studies have reported increasing cases of Hg in the environment⁶ and in humans⁵
2 especially in Asia due to the recent boom in industrial activities in this region. Anthropogenic
3 emissions are either from intentional uses or as byproduct of other activities. At present, coal
4 combustion represents a substantial source of Hg to the environment,⁷ and about half of current
5 emissions are from Asia. Other sources include industrial processes such as cement and chlor-
6 alkali productions, and mining applications, including artisanal and small-scale gold mining.⁶ Hg
7 in the environment finds its way into water and subsequently to soil where it is readily absorbed
8 by aquatic organisms such as fishes and plants, respectively. Hence, reducing the quantity of
9 mercury in effluents before discharge is necessary to reduce the amount of Hg that gets into the
10 environment, and subsequent accumulation in biota.

11 The unique structural and functional properties associated with graphene oxide (GO), such as
12 its high mechanical strength (>1060 GPa), theoretical surface area (about 2600 m² g⁻¹), and the
13 presence of hydroxyl and carboxylic groups are important characteristics that make graphene
14 oxide containing materials suitable for environmental applications.⁸ For instance some authors
15 have employed these properties for adsorption of biphenol A⁹ and arsenic,^{10,11} while others have
16 employed the unique chemical and physical properties of iron magnetic nanoparticles together
17 with other materials in the removal of some toxic substances from solution.^{8,12,13} Iron magnetic
18 nanoparticles have the ease of being removed from solution by magnetization. Iron magnetic
19 nanoparticles synergistically combined with other nanomaterials have very promising capacities
20 for water treatment.

21 With the foregoing in mind, the aim of this study was to covalently combine GO and iron
22 magnetic nanoparticles into one chemical entity at reduced temperature, and employ this new

1 material in the removal/adsorption of Hg^{2+} from aqueous solution. The adsorption data was
2 explained kinetically.

3 **2. MATERIAL AND METHODS**

4 *2.1 Preparation of GO and Synthesis of the APS- Fe_3O_4 hybrid nanoparticles*

5 The chemical exfoliation of natural flake graphite was carried out by modified Hummers'
6 method in which a very long oxidation period was combined with a multi-cycle purification
7 process.⁸ (See supporting information)

8 Fe_3O_4 nanoparticles (FNPs) were prepared using the chemical co-precipitation method by mixing
9 3.0 mL of 1 M FeCl_3 and 1.0 mL of 2 M FeCl_2 (ratio 2:1) solution in a 100 mL beaker containing
10 a magnetic stirring bar. This mixture was continuously stirred under nitrogen while slowly
11 adding 1.0 M aqueous NaOH solution. The initial brown precipitate then turned to a black
12 precipitate (magnetite) while still adding NaOH. The stirrer was turned off and the magnetic
13 stirring bar removed with a strong magnet. The magnetite formed was allowed to settle and the
14 supernatant decanted. The solid was then washed with water and then ethanol accompanied by
15 magnetic decanting after each washing. This is the iron oxide magnetic nanoparticles (FMNP).

16 0.3 g of the synthesized FMNP was then dispersed in 20 mL ethanol by sonication. 3 mL (3-
17 aminopropyl)-trimethoxysilane (APS) was added to the solution with continued sonication for
18 10 min, and then incubated at 60 °C for 4 hr. Enough N-(3-Dimethylaminopropyl)-N'-
19 ethylcarbodiimide hydrochloride (EDC) was added to make 100 mM and the solution sonicated
20 for 5 min. The APS reaction is similar to that adopted by He *et al.*¹⁴

21

22

1 2.2 *Synthesis of GO- Fe₃O₄ nanoparticles*

2 GO magnetic nanoparticles (GOMNP) was synthesized from various concentrations of GO
3 solutions. Solutions containing known amounts of GO were prepared in water and sonicated for
4 5 min (Supporting Information – Table S1). Specific volume of these solutions were added to the
5 APS–Fe₃O₄ mixture above to obtain the final ‘x’ mg ml⁻¹ GO concentration (‘x’ refers to GO
6 concentration which could either be 0.5 or 1.0 mg mL⁻¹; thus representing FMNP:GO
7 concentration ratios of 2:1 and 1:1, respectively) (Table S1). These concentration ratios are
8 denoted as GOMNP-1 and GOMNP-2, respectively. The solutions were mixed, sonicated for 10
9 min. and incubated at 65 °C for 8 hr. The GOMNP particles were then separated by
10 magnetization, washed with water and ethanol thrice, and then freeze dried. Three control pots
11 were set up containing: (a) all reagents but EDC (GOMNP); (b) only FMNP and APS (APS-
12 FMNP); and, (c) FMNP and GO only (GOMNP-0). These were to ascertain the success of the
13 FMNP/APS and FMNP/APS/GO reactions (Table S1).

14 2.3 *Instrumental Characterizations:* The GOMNP particles were characterized by Spectrum
15 One Fourier transform infrared (FTIR) spectrometer (PerkinElmer Instruments Co. Ltd., USA),
16 Pyris Diamond Thermogravimetric/differential thermal analyzer (PerkinElmer Instruments Co.
17 Ltd., USA), Renishaw inVia Raman spectrometer (Renishaw plc, UK), Philips X’Pert PRO X-
18 ray diffraction instrument (PANalytical B.V., Netherlands), and Micromeritics ASAP 2020 M +
19 C accelerated surface area and porosimetry analyzer (Micromeritics Instrument Corporation,
20 USA). Mercury adsorptions were monitored using Varian 710-ES ICP optical emission
21 spectrometer (Supporting Information – S2).

22

23

1 2.5 Mercury adsorption

2 Batch equilibrium adsorption procedure¹⁵ was used to determine the Hg²⁺ adsorption kinetics of
 3 GOMNP. The adsorptions were done at pH 5.0±0.2 for three temperatures – 20, 30 and 40 °C, in
 4 the time range of 5 to 180 minutes using a mercury solution concentration of 50 mg L⁻¹ and 20
 5 mg of the GOMNP–1 each time. The Hg²⁺/GOMNP–1 mixtures were incubated by shaking at
 6 the desired temperature in a temperature controlled shaker during the course of the adsorption
 7 experiment. The tubes were withdrawn from the shaker at the appropriate time interval,
 8 GOMNP–1 in solutions was separated and the Hg²⁺ concentration in the supernatant determined.
 9 The quantity of Hg adsorbed in each case was calculated using equation 1.

$$10 \quad q_e = \frac{(C_o - C_e)V}{M} \quad (1)$$

11 where q_e , C_o and C_e are the amount of Hg adsorbed (mg g⁻¹), the initial and final Hg
 12 concentrations in the solution (mg L⁻¹), respectively; and V (mL) and M (g) are the volume of
 13 solution and mass of GOMNP–1 used for each adsorption, respectively.

14 The simplified linear equations of Lagergren pseudo-first-order – PFO (equation 2), pseudo
 15 second-order – PSO (equation 3) rate models as well as the Elovich (equation 4) and intra-
 16 particle diffusion [16] (equation 5) kinetics models were used to describe the adsorption data.

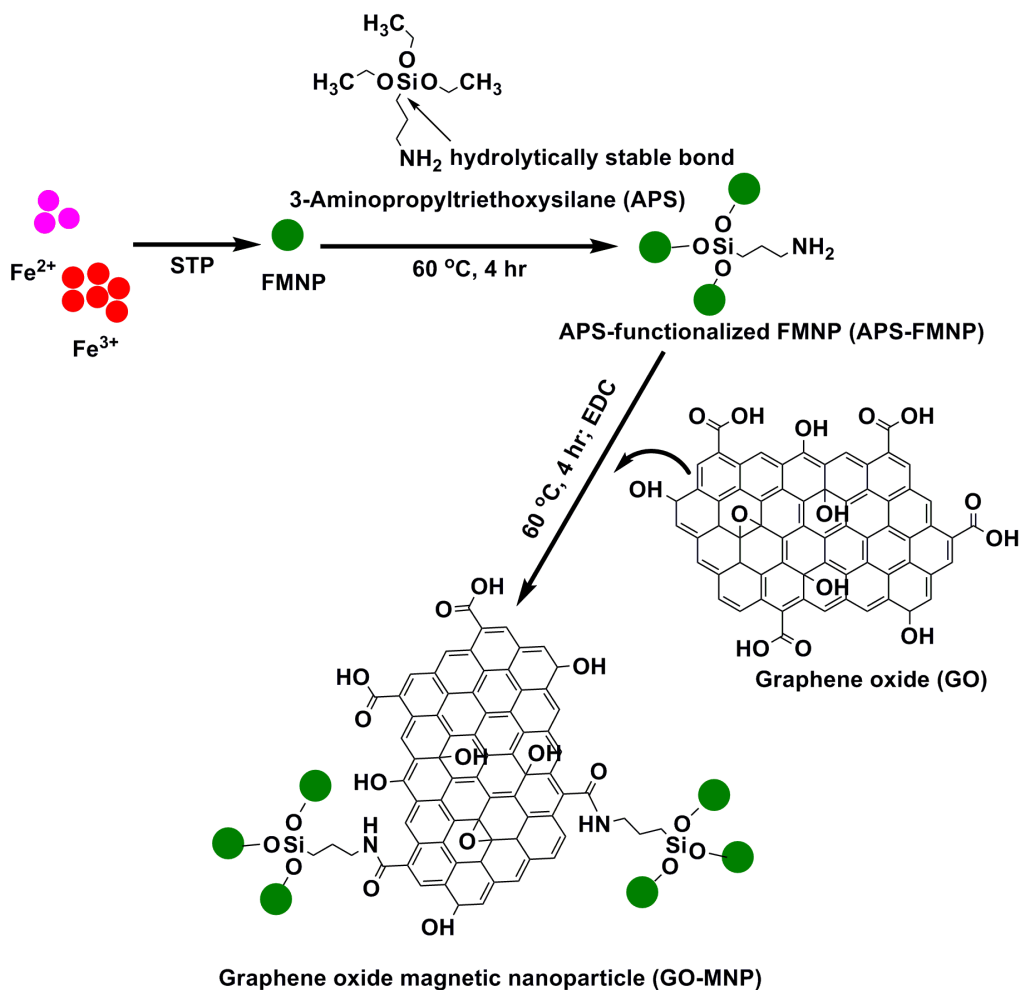
$$17 \quad \log(q_e - q_t) = \log q_e - \frac{k_1}{2.303} t \quad 2$$

$$18 \quad \frac{t}{q_t} = \frac{1}{k_2 q_e^2} + \frac{t}{q_e} \quad 3$$

$$19 \quad q_t = \frac{1}{\beta} \ln(\alpha\beta) + \frac{1}{\beta} \ln(t) \quad 4$$

$$20 \quad q_t = k_i(t^{1/2}) + C \quad 5$$

1 where q_e and q_t are Hg adsorbed (mg g^{-1}) at equilibrium and at time t , respectively; and k_1
 2 (min^{-1}) and k_2 ($\text{g } \mu\text{g}^{-1} \text{min}^{-1}$) are the rate constants of the PFO and PSO, respectively. The q_e and
 3 rate constants were calculated from the slope and intercept of the plots of $\log (q_e - q_t)$ vs. t ; and
 4 $\frac{t}{q_t}$ vs. t for PFO and PSO, respectively, α is the initial adsorption rate ($\text{mg g}^{-1} \text{min}^{-1}$) and β is the
 5 desorption constant (g mg^{-1}) during any one experiment, and C ($\mu\text{g g}^{-1}$) values indicate the
 6 thickness of the boundary layer of Hg^{2+} ion adsorbed, and k_i ($\text{mg/g/min}^{1/2}$) is intra-particle
 7 diffusion rate constant of the control stage.



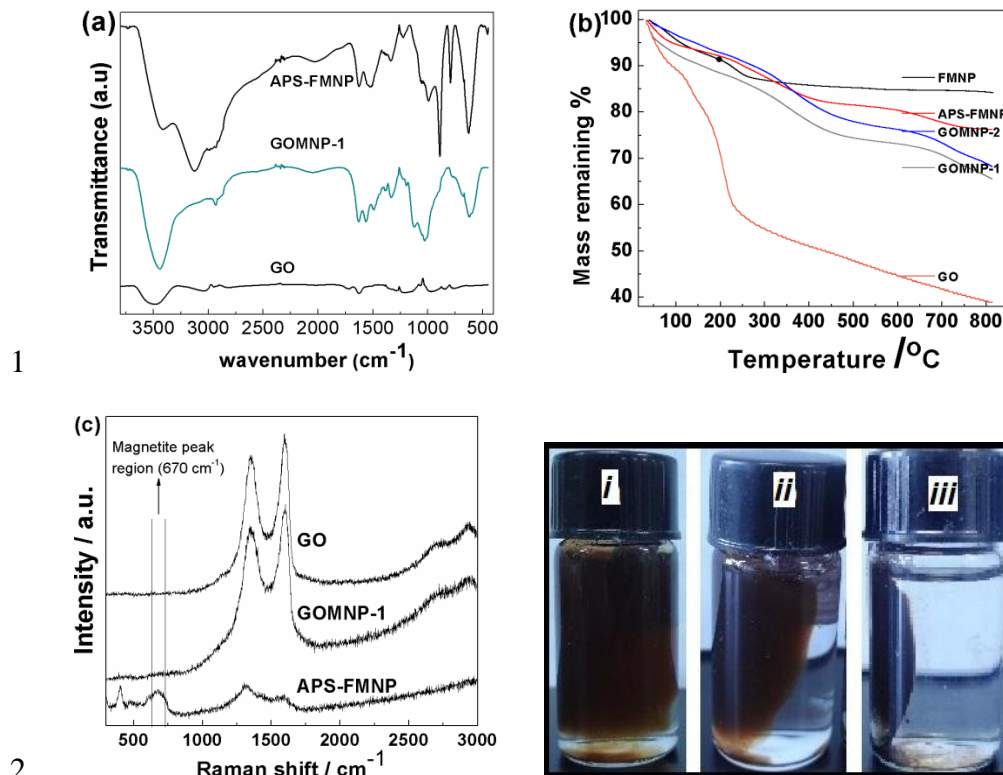
8

9 Figure 1: Schematic synthesis of GOMNP.

1 3. RESULTS AND DISCUSSION

2 3.1 Characterization.

3 The schematic synthesis of the iron magnetic nanoparticles (FMNP) and GO composite is shown
4 in Figure 1. The FMNP particles were first synthesized and then reacted with 3-
5 aminopropyltriethoxysilane (APS), and subsequently GO sheets were attached via the amine
6 group on the APS. This was similar to the modification reaction carried out by He *et al.* [14]
7 Figure 2a shows the IR spectra of GO and the various modified GO–MNPs. The characteristic
8 peaks of pristine GO for hydroxyl groups, $\text{C}=\text{O}$ bond of the amide-I, carboxylate vibrations,
9 and $\text{C}-\text{O}$ band of carboxylic acids were observed at 3436, 1627, 1421, and 1068 cm^{-1} ,
10 respectively.⁸ The IR spectra of various modified GOMNP were different from that of GO as
11 shown in Figure 2a suggesting that the treatment conferred new functional groups unto the GO.
12 In addition to the observed peaks of pristine GO, distinct peaks originating after the treatments
13 were observed in the GOMNP as well as the APS-FMNP. The hydroxyl and amide I band stretch
14 of $\text{C}=\text{O}$ were observed at around 3436 and 1628 cm^{-1} , respectively. However, the GO band at
15 1068 cm^{-1} disappeared with the appearance of three new bands at 890, 1051 and 1129 cm^{-1}
16 indicating the presence of $\text{Si}-\text{O}$ from APS in the newly formed structure. The band around 1330
17 cm^{-1} was attributed to $\text{C}-\text{H}_2$ scissor of the aliphatic propyl chain of the APS while additional
18 bands around 1491 and 1566 cm^{-1} was assigned to the amine $\text{C}-\text{N}$ and $\text{N}-\text{H}$ bend linking APS
19 and GO.¹⁵ The peak close to 600 cm^{-1} was ascribed to absorption by the $\text{Fe}-\text{O}$ bond of the iron
20 oxide. These bands indicate a covalent linkage between GO and the FMNP.¹⁷



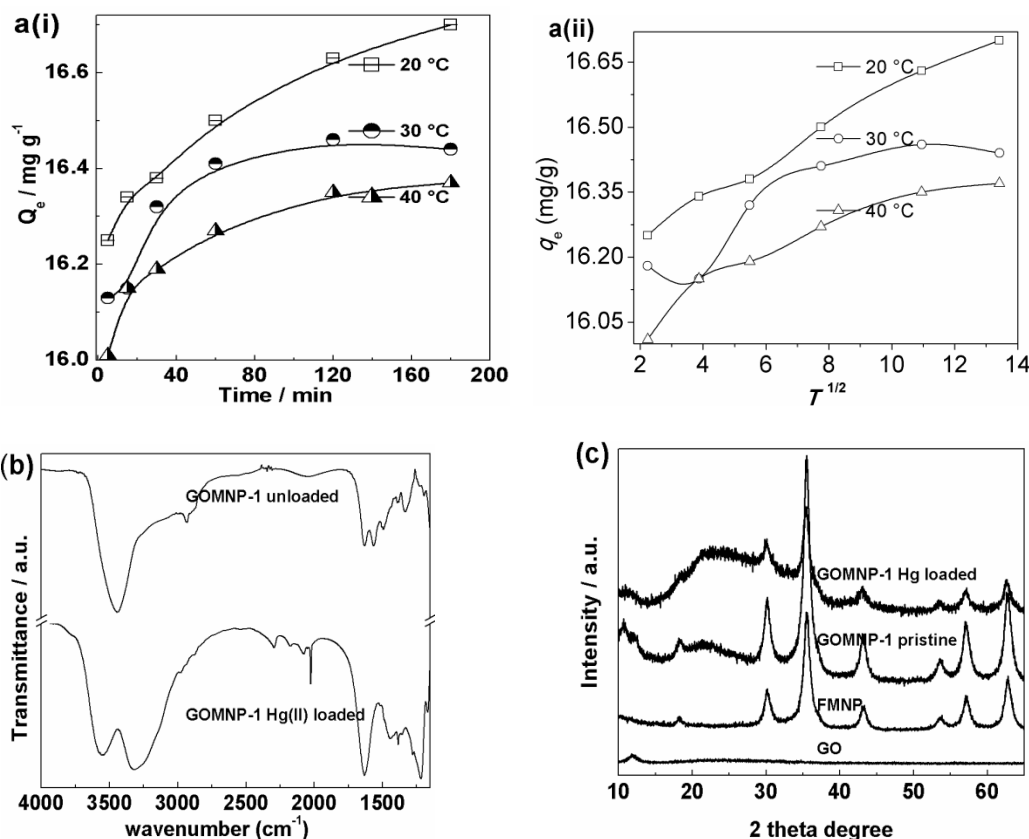
1
2
3 Figure 2. (a) IR spectra of the various synthesized materials; (b) TGA of the GOMNP materials;
4 (c) Raman spectra of GO, APS-FMNP, and GOMNP; (d) magnetic separation from solution test
5 (i) GOMNP-0, (ii) GOMNP and (iii) GOMNP-1.

6 TGA curves of GO, and the various FMNP modifications are shown in Figure 2b. The curve
7 for FMNP showed little weight loss – about 3% below 250°C. Comparing the FMNP with the
8 pristine GO, it was observed that GO showed a far lower thermal stability and much higher
9 weight loss losing about 60 % of its original weight before 380 °C. This weight loss was due to
10 moisture loss at the initial temperature, and later on the pyrolysis and decomposition of the labile
11 oxygen-containing functional groups such as –CO, –OH and –COOH attached to GO resulting
12 in the loss of CO, CO₂ and steam. Further weight loss, which was steady (~5%) occurred
13 thereafter in the temperature range of about 400 to 800°C, and this may be attributed to removal
14 of more stable functional groups at higher temperatures. However, modification of the GO with

1 FMNP reduced the weight loss. The weight loss was between 15 to 25 % depending on the
2 effectiveness of the reaction between GO and FMNP. The higher the quantity of GO attached to
3 FMNP, the more the weight loss. Though magnetic separation test result (Figure 2d) showed that
4 it is possible to react APS–FMNP and GO to obtain GOMNP, comparison of the TGA data of
5 GOMNP, GOMNP–1, and GOMNP–2 showed that higher quantity of GO (up to 5% more) can
6 be attached to FMNP in the presence of EDC; thus, more GO was linked per gram FMNP in the
7 presence of EDC.

8 Raman spectroscopy is another method for the identification of the presence of carbonaceous
9 materials as well as iron oxide phase in a compound because of the varying vibrational
10 fingerprints of magnetite, maghemite and hematite. Raman spectra of the GO and the modified
11 GOMNPs showed the presence of the added carbonaceous materials in the GOMNPs (Figure
12 2c). GO and GOMNP-1 displayed the well known *D*- and *G*-bands associated with GO
13 materials at around 1354 and 1600 cm^{-1} , respectively. The *D* peaks were attributed to the
14 presence of condensed benzene regions in the graphene structure, while the *G* peaks were
15 evidence of sp^2 bonded carbon that is present in planar sheet configurations which includes sp^2
16 C=C stretch vibrations.⁸ The spectra of APS-FMNP and GOMNP showed additional peak at 670
17 cm^{-1} which corresponds to that of magnetite. The BET surface areas and porosities of GO,
18 FMNP and GOMNP-1 were determined as 56, 125 and 214 $\text{m}^{-2} \text{g}^{-1}$, respectively; and adsorption
19 average pore diameters of 4.8, 13.7, and 13.1 nm, respectively (Supporting Information – Figure
20 S1). The observed increases in surface area of these new materials were attributed to the rigid
21 nature of the FMNP particles which reduces stacking of the GO sheets; and hence increases the
22 surface area.

1 To ascertain whether the magnetic property of the FMNP were transferred to GOMNP by the
2 FMNP attachment to the GO surface via the amine group of the 3-aminopropyltriethoxysilane
3 (APS), GOMNP, GOMNP-0 and GOMNP-1 were subjected to magnetic separation test. If the
4 GO sheets are attached to the FMNP, separation will be perfect in the presence of external
5 magnetic field. After 20 min, it was observed that GOMNP and GOMNP-1 were separated as
6 shown in Figure 2d. However, the GOMNP-0 (Figure 2di) remained unseparated just like before
7 the application of the external magnetic field and no clear solution was observed indicating that
8 GO-magnetic hybrid particles were not formed like in the GOMNP and GOMNP-1. For
9 GOMNP (Figure 2dii) partial separation was observed, while GOMNP-1 (Figure 2diii), on the
10 other hand, showed a complete separation. This was an indication that the FMNPs were attached
11 to the GO and were separated along with the GO sheets. GO were covalently attached to the
12 FMNP via amide bonds which were formed between the amine group of APS and the carboxylic
13 group of the GO sheets. He *et al.*¹⁴ have reported a similar reaction using APS.



1

2

3 Figure 3 a(i). effect of time on Hg^{2+} adsorption by GOMNP-1; a(ii). non-linear curves of the
 4 intra-particle diffusion kinetics model at the various temperatures studied; (b) IR spectra of Hg^{2+}
 5 loaded and pristine GOMNP; (c) XRD patterns of GO, FMNP, Pristine GOMNP-1, and
 6 GOMNP-1 loaded with Hg^{2+} .

7

8 3.2 Adsorption kinetics of Mercury.

9 Batch equilibrium adsorption procedure was used to study the Hg^{2+} adsorption kinetics of
 10 GOMNP-1 at pH 5.0 ± 0.2 and at 20, 30, and 40 °C using Hg^{2+} concentration of 50 mg L⁻¹ and 20
 11 mg of GOMNP-1 in the time range of 5 to 180 minutes. Adsorption kinetics study is important
 12 because it gives information on the rate of the adsorption of a particular sorbate under a set of
 13 prescribed conditions. Preliminary investigations conducted to compare the Hg^{2+} adsorption
 14 capacity of pristine GO and GOMNP-1 showed that GO has Hg^{2+} adsorption capacity of 2.9 mg

1 g^{-1} while GOMNP-1 has over 5 fold higher adsorption capacity. The adsorption time curve
2 (Figure 3a(i)) showed that Hg^{2+} adsorption equilibria were fast and this was reached within 120
3 minutes. Similar fast adsorption results have been reported in literature for graphene based
4 materials.^{10,17,18} The difference in adsorption capacities of GO and GOMNP-1 is an indication
5 that in addition to the adsorption sites on the GO sheets provided by the presence of the
6 carboxylic ($-\text{COO}$) and hydroxyl ($-\text{OH}$) functional groups, the FMNP particles magnetic acted
7 as sorbent for Hg^{2+} in solution. The significant difference in the Hg^{2+} adsorption capacities of
8 both GO and GO/FMNP composites is also testimony to the success of attaching GO to the
9 FMNP particles. Figure 3a(i) also showed that increase in Hg^{2+} solution temperature from 20 to
10 40 °C did not lead to a corresponding increase in adsorption capacity, but that adsorption
11 capacity is inversely proportional to the temperature. The adsorption trend is 20 °C > 30 °C > 40
12 °C. The negative effect of temperature on the adsorption of Hg^{2+} by the GOMNP-1 material may
13 be an indication that the process occurs mainly by physisorption and is exothermic. Vidic and
14 Siler² and Olsen *et al.*⁷ have also reported similar temperature effect on Hg^{2+} adsorption. This
15 observation could be explained thus: Hg metal is liquid and volatile at room temperature;
16 increasing the adsorption medium temperature increases the kinetic energy of the molecules in
17 solution and subsequently the molecules moves away from the adsorption surfaces, and hence
18 the observed reduction in adsorption with increase in temperature.

19

20

21

22

23

1 Table 1: Adsorption kinetics model parameters at 20, 30, and 40 °C

Kinetics model	Model parameters	Temperatures		
		20 °C	30 °C	40 °C
pseudo-first-order	q_e (mg g ⁻¹)	2.76	2.08	1.67
	K_1 (min ⁻¹)	0.007	0.002	0.002
	r^2	0.909	0.720	0.869
pseudo-second-order	q_e (mg g ⁻¹)	-*	-	-
	K_2 (g mg ⁻¹ min ⁻¹)	-	-	-
	r^2	0.922	0.522	0.154
Elovich	q_e (mg g ⁻¹)	16.61	16.43	16.33
	β	7.87	10.75	10.00
	r^2	0.950	0.851	0.990
Intra-Particle diffusion	C (mg g ⁻¹)	16.17	16.12	16.00
	K_i	0.04	0.03	0.03
	r^2	0.990	0.800	0.917

2 * values are less than 0.001

3 The Hg²⁺ adsorption data at 20, 30, and 40 °C was fitted to four kinetics models: the pseudo-
4 first order, pseudo-second order, Elovich and intra-particle diffusion kinetics models (Table 1).
5 These models were used to describe the adsorption as well as predict the adsorption
6 mechanism(s) involved in the uptake of Hg²⁺ by GOMNP-1. Data from Table 1 indicated that
7 the Lagergren pseudo-first order kinetics described the adsorption better than the Lagergren
8 pseudo-second order kinetics model as revealed by the correlation coefficients (r^2) values.
9 However, none of these models were able to predict the adsorption capacity of the GOMNP-1

1 material, nor could they be used to confidently predict the adsorption mechanism that controlled
2 the adsorption process of Hg^{2+} on GOMNP-1.

3 The r^2 values of the Elovich kinetics model on the other hand showed that the adsorption data
4 fitted the model better than the pseudo-first order and pseudo-second order kinetics models. The
5 Elovich model was able to predict the adsorption capacity of the GOMNP for the sorbate. This
6 adsorption model which originated from chemical reaction kinetics suggested that there was
7 some degree of boundary layer control between the Hg^{2+} ions and the GOMNP-1 surface active
8 adsorption sites since the curves does not pass through the origin (Supporting Information –
9 Figure S2 a, b, c). This boundary layer control is related to the rate determining mechanism and
10 involved valence electron forces through sharing of electrons between the Hg^{2+} and GOMNP-1
11 surface active adsorption sites.¹⁹

12 The adsorption kinetic data were further processed to determine whether intra-particle
13 diffusion was the rate limiting step of the adsorption and to find rate parameters for the model
14 (Table 1 and Figure 3a(ii)). The r^2 values of the intra-particle diffusion model were all relatively
15 better than those of other studied models (>0.800) and the C ($\mu\text{g g}^{-1}$) values of this model, an
16 indication of the boundary layer thickness of Hg^{2+} on the adsorbent surface, showed that the
17 Hg^{2+} removal process was mainly surface phenomenon (adsorption) occurring by physisorption.
18 This conclusion was reached because the quantity of Hg^{2+} on the adsorbent surface significantly
19 correlated to the experimental values. At lower temperature ($20\text{ }^\circ\text{C}$), the r^2 value of the pseudo-
20 second-order kinetics was higher than that of the pseudo-first-order kinetics. The high r^2 values
21 of intra-particle diffusion and pseudo-second-order kinetics models support the assertion that the
22 overall rate of the adsorption process was controlled by more than one-step as observed from the
23 non-linear curves of Figure 3a(ii). However, as ambient temperature increased, the adsorption

1 mechanism changed; the r^2 values of the intra-particle diffusion model at higher temperatures (20
2 and 30 °C) were close to unity and also significantly higher than those of both the pseudo-first-
3 and -second-order kinetics. This indicated that as temperature increased the intra-particle
4 diffusion was the predominant rate determining step of Hg^{2+} adsorption on the GOMNP-1
5 surface. This was evident in the shapes of the intra-particle diffusion model curves in Figures
6 3a(ii) at 30 and 40 °C. Hence, different kinetics mechanisms control Hg^{2+} at different solution
7 temperatures.

8 The infra-red spectra of the Hg^{2+} -loaded and unloaded GOMNP-1 were compared (Figure
9 3b). It was observed that the Hg^{2+} -loaded GOMNP-1 spectra showed shifts in spectra peaks
10 (especially for the carboxylate and hydroxyl groups) as well as new spectra bands. The amide-I
11 band at 1628 shifted to 1632 cm^{-1} , while the hydroxyl vibration at 1491 cm^{-1} shifted to 1442 cm^{-1} .
12 However, there was a peak split at 3436 cm^{-1} resulting into two new peaks observed at 3324
13 and 3551 cm^{-1} . These peaks were attributed to the adsorption of Hg^{2+} on the hydroxyl functional
14 group. These peak shifts and new bands associated with hydroxyl vibrations and amide-I bands,
15 have been attributed to the counter ions changes associated with these functional groups anions
16 after the adsorptions of Hg^{2+} ; and are indications of the role played by these functional groups on
17 the GOMNP-1 surface.

18 The crystal phase compositions of the pristine FMNP, GO, GOMNP-1 as well as the Hg^{2+}
19 loaded GOMNP-1 were studied by powder X-ray diffraction (**Figure 3c(i-iv)**). The analysis of
20 X-ray patterns revealed structural changes that occurred after specific reactions/adsorption. GO
21 (**Figure 3ci**) showed a strong peak around $2\theta=12^\circ$ and a weak broad peak around 23° . Both
22 peaks indicated the presence of functional groups containing oxygen which was formed during
23 the strong graphite oxidation process.²⁰ The pristine GOMNP-1 XRD diffractions (**Figure 3ciii**)

1 showed the characteristic peaks associated with the presence of pure spinal structures of Fe_3O_4
 2 (**Figure 3civ**) at 2θ values of 30.1, 35.5, 43.1, 53.6, 57.1 and 62.7° , with the respective indices of
 3 (220), (311), (400), (422), (511), and (440), as well as the GO diffraction bands discussed earlier.
 4 These observations above indicated that the formation of the GOMNP-1 did not result in phase
 5 change of Fe_3O_4 . As similarly observed in the IR spectra, there was a shift in the diffraction
 6 pattern of the GOMNP-1 after Hg^{2+} adsorption (**Figure 3cii**). All FMNP and GO 2θ observed
 7 bands were also present in the Hg^{2+} -loaded GOMNP-1. However, the GO diffraction band
 8 around $2\theta=23^\circ$ became broadened. This was attributed to the presence of Hg^{2+} which caused a
 9 distortion in the crystal structure of the GOMNP-1 within that band area; and since that band
 10 area has been attributed to GO; this suggested that Hg^{2+} adsorptions occurred on the GO sheets.

11 Comparisons of GOMNP-1 Hg^{2+} adsorption capacity, q_e , to those of GO modified with
 12 metal/metal oxide in literature (Table 2) showed that the GOMNP-1 had a better q_e value.

13 Table 2: Comparison of Hg^{2+} adsorption q_e on GOMNP-1 with GO modified with metal/metal
 14 oxide

Adsorbent	q_e (mg/g)	Reference
GOMNP	16.6	present study
RGO-MnO ₂	9.0	(Sreeprasad <i>et al.</i> , 2011) [17]
RGO-Ag	9.0	(Sreeprasad <i>et al.</i> , 2011) [17]
GO	2.9	present study

15

16 4. CONCLUSION

17 The kinetics of Hg^{2+} adsorption by graphene oxide-iron oxide magnetic nano-particles
 18 composite (GOMNP) was investigated. Iron oxide magnetic nano-particles was attached to the
 19 graphene oxide (GO) using 3-aminopropyltriethoxysilane at a considerably low temperature. The

1 GO-magnetic nanoparticles composite has over 5-fold higher adsorption capacity than the
2 pristine GO sheets. Increase in temperature had a negative effect on the adsorption of Hg^{2+} by
3 the composite: $20\text{ }^\circ\text{C} > 30\text{ }^\circ\text{C} > 40\text{ }^\circ\text{C}$. The Elovich kinetics model described the Hg^{2+} adsorption
4 better than pseudo first- and -second order kinetics models. Hg^{2+} adsorption kinetics mechanism
5 at $20\text{ }^\circ\text{C}$ is predominantly the pseudo-second order kinetics while at higher temperatures the
6 mechanism was predominantly intra-particle diffusion. IR spectra analysis showed that hydroxyl
7 and carboxylate functional groups were mainly responsible for Hg^{2+} adsorption. XRD diffraction
8 patterns also confirmed the involvement of GO functional groups in the adsorption. GOMNP is
9 thus a promising nanosorbent for Hg^{2+} removal from aqueous solutions.

10

11 **ACKNOWLEDGEMENTS**

12 The financial support of the National Science Foundation of China (Grants no. 91023001 and
13 60911130231) and the Chinese Academy of Sciences (Knowledge Innovation Program, Grant
14 no. KJCX2-YW-H21) is acknowledged. We also acknowledge the supports of Chief S.L.
15 Edu/Chevron Research grant (Nigeria Conservation Foundation) Nigeria, and the World
16 Academy of Sciences (TWAS), Trieste Italy and the Chinese Academy of Sciences (CAS),
17 China for the award of CAS-TWAS Postgraduate Fellowship (FR number: 3240255024) to P. N.
18 Diagboya; late Mrs. Rebecca A. Okoh, and Mr. Victor P.O. Okoh, Department of Estate
19 Management, School of Environmental Sciences, Yaba College of Technology, Lagos Nigeria.

20

21 **SUPPORTING INFORMATION AVAILABLE.**

22 Further information on the synthesis of GO-MNP; descriptions of materials and methods used;
23 BET diagram; and the Elovich kinetics isotherms at 20, 30, and $40\text{ }^\circ\text{C}$.

1 **REFERENCES**

- 2 1. Y.S. Hong, Y.M. Kim, K.E. Lee, *J Prev. Med. Public Health*, 2012, **45**, 353-63.
- 3 2. R.D. Vidic, D.P. Siler, *Carbon*, 2001, **39**, 3-14.
- 4 3. WHO (World Health Organization), *Guidelines for Drinking-Water Quality*, 4th ed. Geneva:
5 World Health Organization. xxiii, 2011, pp. 541.
- 6 4. Y.D. Jing, Z.L. He, X.E. Yang, *Chemosphere*, 2007, **69**, 1662-1669.
- 7 5. S.R. Shin, A.L. Han, *Korean J Fam. Med.*, 2012, **33**, 320-325.
- 8 6. E.M. Sunderland, N.E. Selin, *Sunderland and Selin Environmental Health*, 2013, **12**, 2.
- 9 7. E.S. Olson, S.J. Miller, R.K. Sharma, G.E. Dunham, S.A. Benson, *J. Haz. Mat.*, 2000, **74**, 61-
10 79.
- 11 8. P.N. Diagboya, B.I. Olu-Owolabi, D. Zhou, B.H. Han, *Carbon*, 2014, **79**, 174–182.
- 12 9. J. Xu, L. Wang, Y. Zhu, *Langmuir*, 2012, **28**, 8418-8425.
- 13 10. V. Chandra, J. Park, Y. Chun, J.W. Lee, I.C. Hwang, K.S. Kim, *ACS Nano.*, 2010, **4**, 3979-
14 86.
- 15 11. A.K. Mishra, S. Ramaprabhu, *Desalination* 2011, **282**, 39-45.
- 16 12. S.R. Kanel, D. Nepal, B. Manning, H. Choi, *J. Nanoparticle Res.*, 2007, **9**, 725-735.
- 17 13. I.N. Savina, C.J. English, R.L. Whitby, Y. Zheng, A. Leistner, S.V. Mikhalovsky, et al., *J.*
18 *Haz. Mater.*, 2011, **192**, 1002-1008.
- 19 14. F. He, J. Fan, D. Ma, L. Zhang, C. Leung, H.L. Chan, *Carbon*, 2010, **48**, 3139-3144.
- 20 15. P.N. Diagboya, B.I. Olu-Owolabi, K.O. Adebawale, *J Environ Manag.*, 2014, **146**, 42–49.
- 21 16. B.I. Olu-Owolabi, P.N. Diagboya, K.O. Adebawale, *J Environ Manag.*, 2014, **137**, 1–9.
- 22 17. T.S. Sreeprasad, S.M. Maliyekkal, K.P. Lisha, T. Pradeep, *J. Haz. Mater.*, 2011, **186**, 921-
23 931.

- 1 18. V. Chandra, K.S. Kim, Chem Commun.(Camb), 2011, **47**, 3942-3944.
2 19. B.I. Olu-Owolabi, P.N. Diagboya, W.C. Ebaddan, Chem. Eng. J., 2012, **195–196**, 270–275.
3 20. C. Wu, Q. Cheng, S. Sun, H.B. Han, Carbon 2012, **50**, 1083–1089.

4

5

FIGURES AND TABLES LEGEND

6

LIST OF FIGURES

7 Figure 1: Schematic synthesis of GOMNP.

8 Figure 2. (a) IR spectra of the various synthesized materials; (b) TGA of the GOMNP materials;
9 (c) Raman spectra of GO, APS-FMNP, and GOMNP; (d) magnetic separation
10 from solution test (i) GOMNP–0, (ii) GOMNP and (iii) GOMNP–1.

11 Figure 3 a(i). effect of time on Hg^{2+} adsorption by GOMNP–1; a(ii). non-linear curves of the
12 intra-particle diffusion kinetics model at the various temperatures studied; (b) IR
13 spectra of Hg^{2+} loaded and pristine GOMNP; (c) XRD patterns of GO, FMNP,
14 Pristine GOMNP–1, and GOMNP–1 loaded with Hg^{2+} .

15

16

LIST OF TABLES

17 Table 1: Adsorption kinetics model parameters at 20, 30, and 40 °C

18 Table 2: Comparison of Hg^{2+} adsorption q_e on GOMNP–1 with GO modified with
19 metal/metal oxide.